HHS Public Access

Author manuscript

ACS Chem Biol. Author manuscript; available in PMC 2022 February 19.

Published in final edited form as:

ACS Chem Biol. 2022 February 18; 17(2): 314–321. doi:10.1021/acschembio.1c00745.

Bifunctional Peptide that Anneals to Damaged Collagen and Clusters TGF-β Receptors Enhances Wound Healing

Sayani Chattopadhyay[†], **Leandro B. C. Teixeira**[‡], **Laura L. Kiessling**[†,§,⊥], **Jonathan F. McAnulty**[#], **Ronald T. Raines**[*,†,§,⊥]

[†]Department of Chemistry, University of Wisconsin–Madison, Madison, Wisconsin 53706, United States

[‡]Department of Pathobiological Sciences, School of Veterinary Medicine, University of Wisconsin–Madison, Madison, Wisconsin 53706, United States

[§]Department of Biochemistry, University of Wisconsin–Madison, Madison, Wisconsin 53706, United States

[#]Department of Surgical Sciences, School of Veterinary Medicine, University of Wisconsin–Madison, Madison, Wisconsin 53706, United States

[⊥]Department of Chemistry, Massachusetts Institute of Technology, Cambridge, Massachusetts 02139, United States

Abstract

Transforming growth factor-β (TGF-β) plays important roles in wound healing. The activity of TGF-β is initiated upon the binding of the growth factor to the extracellular domains of its receptors. We sought to facilitate the activation by clustering these extracellular domains. To do so, we used a known peptide that binds to TGF-β receptors without diminishing their affinity for TGF-β. We conjugated this peptide to a collagen-mimetic peptide that can anneal to the damaged collagen in a wound bed. We find that the conjugate enhances collagen deposition and wound closure in mice in a manner consistent with the clustering of TGF-β receptors. This strategy provides a means to upregulate the TGF-β signaling pathway without adding exogenous TGF-β and could inspire means to treat severe wounds.

Graphical Abstract

[*]**Ronald T. Raines** – *Department of Chemistry, Massachusetts Institute of Technology, Cambridge, Massachusetts 02139, United States;* rtraines@mit.edu.

Sayani Chattopadhyay – *Department of Chemistry, University of Wisconsin–Madison, Madison, Wisconsin 53706, United States*

Leandro Teixeira – *Department of Pathobiological Sciences, School of Veterinary Medicine, University of Wisconsin–Madison, Madison, Wisconsin 53706, United States*

Laura L. Kiessling – *Department of Chemistry, Massachusetts Institute of Technology, Cambridge, Massachusetts 02139, United States*

Jonathan F. McAnulty – *Department of Surgical Sciences, School of Veterinary Medicine, University of Wisconsin–Madison, Madison, Wisconsin 53706, United States*

The authors declare no competing financial interest.

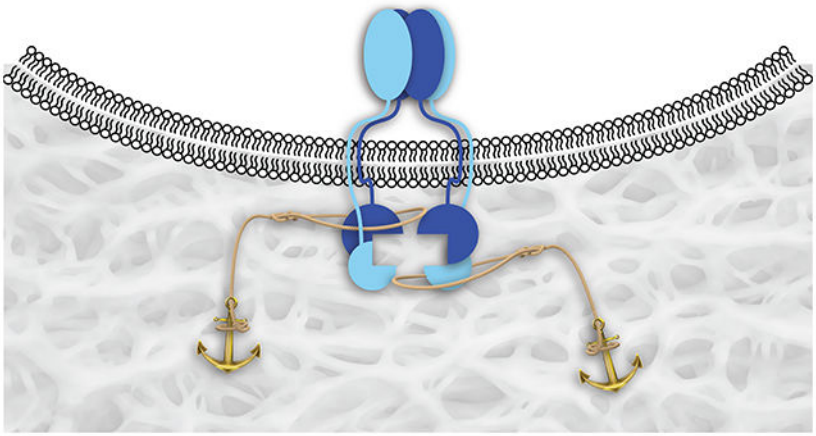

INTRODUCTION

The transforming growth factor β (TGF-β) family is a group of mammalian secretory proteins that play myriad roles in development and disease.[1–4] Their biological activities are initiated upon interaction with two type-I receptors (TβRI) and two type-II receptors (TβRII).[5–7] These cell-surface receptors are characterized by an extracellular TGF-β–binding domain, a transmembrane domain, and a cytosolic serine/threonine kinase domain.[8] Upon binding to TGF-β, TβRII recruits TβRI into an activated heterotetrameric complex (Figure 1A). The cytosolic domain of TβRII then catalyzes the phosphorylation of the regulatory region of TβRI and thereby activates the adjacent serine/threonine kinase domain, ultimately leading to the phosphorylation of downstream effectors, Smad2 and Smad3, which translocate to the nucleus and mediate gene expression.

Activation of the TGF-β signaling cascade can promote dermal fibrosis.[9–13] For example, TGF-β administered to full-thickness wounds in rabbits by encapsulation in a collagen-sponge scaffold accelerates re-epithelialization and contraction.[14] Similarly, TGF-β applied topically or by injection heals wounds by increasing tensile strength and promoting fibroblast proliferation and collagen deposition.[15–20] These approaches, however, require the administration of exogenous TGF-β, which can have deleterious consequences.[9–12]

Using phage display, we identified dodecapeptides that bind to the extracellular domains of both TβRI and TβRII to form complexes with $K_d \approx 10^{-5}$ M.[21] These peptides do not, however, antagonize the binding of TGF-β. In addition, we demonstrated that a multivalent display of these ligands on a PEG-based dendrimer increases their functional efficacy for the receptors.[21] Likewise, immobilization of the ligands on a synthetic surface enables activation by subpicomolar concentrations of endogenous TGF-β.[22] Gene expression profiles revealed that the surfaces regulate TGF-β–responsive genes selectively. Now, we sought to exploit these ligands in vivo.

Collagen is the major component of the extracellular matrix (ECM).[23–25] We and others have reported on the use of collagen-mimetic peptides (CMPs) to anchor probes and growth factors in damaged or abnormal collagen.[26–35] Here, we use a CMP conjugate to immobilize

a peptidic ligand for TGF-β receptors in wound beds of mice. Our intent is to cluster cell-surface TβRI and TβRII and thereby enhance the sensitivity of cells to circulating TGF-β (Figure 1B). As TGF-β is involved in various stages of wound healing,[9–12] we validate the efficacy of our approach by using a variety of assays.

RESULTS AND DISCUSSION

Peptide Design.

As an effector to sensitize cell-surface receptors to TGF-β signaling, we used the LTGKNFPMFHRN peptide.[21] As a CMP, we chose $(PPG)_7$ because of its simplicity and demonstrated efficacy in relevant contexts in vitro, ex vivo, and in vivo.[26,28,30,33,34] (We note that the use of a CMP containing 4-fluoroproline residues could be advantageous in future studies.[29,31,36]) In its initial discovery, LTGKNFPMFHRN (**Tβrl**) was displayed as a fusion to the N-terminus of the PIII coat protein of phage.[21] We mimicked this display by conjugating **Tβrl** to the N-terminus of **CMP**. Accordingly, we synthesized the 33-mer peptide **Tβrl–CMP** and its **Tβrl** and **CMP** components by solid-phase peptide synthesis (SPPS).

Mouse Model.

Wound healing is a complex process. Mouse models have illuminated the mechanisms that underlie wound healing and established translatable therapeutic strategies.[37–40] We chose to use diabetic (*db*/*db*) mice as our model. These mice exhibit characteristics similar to those of adult human onset type II diabetes mellitus,[41,42] including impaired wound healing.[43] Excisional wounds in *db*/*db* mice show a delay in wound closure, decreased granulation tissue formation, decreased vascularization in the wound bed, and diminished cell proliferation.[44] The course of wound healing in these mice follows closely the clinical observations of human diabetic patients.[45] For example, these mice show delayed and reduced expression of keratinocyte growth factor and peripheral neuropathy,[46] as do diabetic humans.[47]

We employed an excisional wound model, which heals from the wound margins and provides the broadest assessment of the various parameters for wound healing, such as re-epithelialization, fibrovascular proliferation, contracture, and angiogenesis.[38] This wound model also offers large dorsal surfaces that simplify the application of topical agents directly into the wound bed and provides two wounds side-by-side on the same mouse.

Unsplinted Wounds.

Wounds were created in the craniodorsal region of *db*/*db* mice under anesthesia and treated topically with **Tβrl–CMP** (25 μL of a 20 mM solution in 5% PEG/saline solution).[48,49] **CMP** and **Tβrl** (25 μL of 20 mM solutions in 5% PEG/saline) were also tested individually. The delivery vehicle itself was tested as a control.

The fibrovascular influx and the deposition of new collagen in wounds were measured by examining the picrosirius red-stained histologic sections under polarized light[50] and expressed as a percentage of the total wound area. The picrosirius red stain highlights

the areas of new collagen deposition, as well as extant dermal collagen. Due to more extensive crosslinking and maturation, older collagen is stained more brightly and densely in comparison to the newly formed collagen. Upon its release from degranulating platelets, TGF-β1 can attract fibroblasts chemotactically to a wound site[51–53] and stimulate their proliferation.[54] As part of a positive feedback mechanism, fibroblasts release additional TGF-β in response and promote collagen biosynthesis.

Compared to the control wounds treated with **Tβrl**, **CMP**, or the delivery vehicle, wounds exposed to **Tβrl–CMP** exhibited a significant increase in the amount of collagen deposited in the wound bed. (Figure 2A). This result is consistent with reports in which the topical application of TGF-β in animal models enhanced the production of collagen and fibronectin by fibroblasts[55,56] and potently stimulated granulation tissue formation in wound-healing models.[57,58] In contrast, the production of collagen was diminished in the presence of anti–TGF-β antibodies.[59]

The wound-healing process is associated with the transient accumulation of fibroblasts that express elevated levels of TβRI and TβRII.[15–20] The highest cellular density is observed in the deepest regions of the granulation tissue.[60] **Tβrl–CMP** tethered to the wound bed is poised to preorganize these receptors and thereby enhance the cellular sensitivity to TGF-β signaling and consequent formation of new collagen, without a need for exogenous TGF-β (Figure 1). Earlier work showed that tethering TGF-β to a PEG-based polymer scaffold caused a significant increase in matrix production and collagen deposition.[61] Such a treatment also counteracted the attenuation of ECM production, which is observed otherwise in the presence of biomaterials containing cell-adhesive ligands.[62] The **Tβrl–CMP** conjugate can behave in a similar manner and promote cellular adhesion while strengthening the wound bed itself by enhancing collagen synthesis and consequent ECM production. **Tβrl** alone cannot, however, access such preorganization and provides a response that is indistinguishable from that of the delivery vehicle (Figure 2A).

A similar outcome was apparent when wounds were analyzed for an inflammatory response. The concentration of TGF-β is ~1 pM in human serum.[63] Upon cutaneous injury, TGF-β levels elevate rapidly.[64,65] For example, TGF-β levels reach a peak at 3 days post 6-mm full-thickness wounding in transgenic mice, which coincides with the peak of the inflammation during early stages of wound healing.[65] Subcutaneous injection of TGF-β affords a histological pattern for neutrophil and macrophage recruitment, fibroblast proliferation, and vascular growth, similar to the process of normal inflammation and repair in cutaneous wounds.[57] In early stages, TGF-β is a highly chemotactic ligand for human peripheral blood monocytes,[66] which is critical for the initiation of an inflammatory response. Through a positive feedback mechanism, the recruited monocytes and macrophages produce more TGF-β (thereby perpetuating their activity) as well as mitogenic and chemotactic substances that act on other cells. Wounds treated with **Tβrl–CMP** showed an inflammatory influx significantly greater than that of **Tβrl**, **CMP**, or the delivery vehicle (Figure 2B). The macrophages once activated or during maturation, downregulate their receptors for TGF-β and hence their ability to be stimulated further.[66] The peripheral blood monocytes also become susceptible to deactivation by TGF-β,[67] which inhibits the proteolytic environment creased by inflammatory cells and eases the healing process into a proliferative phase.[68]

Re-epithelialization is the process by which keratinocytes both proliferate and migrate from wound edges to create a barrier over the wound.[69] The role of TGF-β in this process is not completely understood. In vitro, TGF-β inhibits the proliferation of keratinocyte but enhances their migration.[70,71] Data in vivo are contradictory. Transgenic mice that overproduced TGF-β show enhanced epithelialization in partial-thickness wounds,[72] and anti–TGF-β antibodies administered to rabbits impair epithelialization.[73] On the other hand, mice null for Smad3 show accelerated keratinocyte proliferation and epithelialization upon the administration of TGF-β compared to wild-type mice.[52,74] In our experiment, we observed a tendency towards increased epithelialization of wound beds treated with **Tβrl–CMP** (Figure 2C). This result is consistent with the cells responding quickly to endogenous TGF-β, which modulates the proliferative and migratory properties of the keratinocytes.[70,71]

No discernible differences were apparent in the rate of wound closure in the treated wounds (Figure 2D). This equivalence could be due to the preponderance of wound closure by contracture in rodents. That obscures wound changes related to epithelial closure or from the formation of scabs, whose removal disturbs the newly formed epidermis and could make wound size measurements inconclusive. We therefore took an alternative, complementary experimental approach.

Splinted Wounds.

Mouse skin models are informative but dissimilar from human skin models in that their major mechanism of wound closure is contraction; in humans, re-epithelialization and granulation tissue formation are the major phases.[37–39,40,69] The use of splints around excisional wounds in mice forces healing to occur by granulocyte formation and re-epithilialization, while minimizing the effects of contraction compared to those in unsplinted wound models.[75] As described previously,[28] we sutured silicone O-rings around the wound margins to act as splints. We increased the cohort size to eight mice per group. Wounds were treated with 25 μL of **Tβrl–CMP**, **Tβrl**, **CMP**, or the delivery vehicle, as with the unsplinted wounds. The wounded mice were then allowed to recover and monitored over a period of 16 days.

Histopathological analysis post-euthanasia on day 16 revealed that 15 of the 16 wounds treated with **Tβrl–CMP** were closed completely (Figure 3). Likewise, the wound size was significantly lower than that for the delivery vehicle (Figure 4A). Treatment with **Tβrl** also showed a slightly enhanced wound closure, though it was not significantly different from that for the delivery vehicle and comparable to that for treatment with **CMP**. Upon comparing the extent of re-epithelialization, we noticed improved keratinocyte proliferation in the wound beds treated with **Tβrl–CMP** in comparison to that in the wounds treated with **CMP** or the delivery vehicle (Figure 4B). TGF-β has been reported to promote epithelial cell attachment and migration in vivo[76,77] and to stimulate the expression of keratinocyte integrins during re-epithelialization.[78] Keratinocyte migration takes place across a substrate, typically the dermis. The deposition of a substantial granulation tissue layer over the longer time period of the splinted-wound experiments (16 days), could have provided the requisite surface for the migration of keratinocytes and increased the length of newly formed epithelial layer.

Dose–Response Analyses.

Finally, we assessed the potency of the TGF-β receptor ligand in ECM formation by treating the wounds with increasing doses of **Tβrl–CMP**. Identical 6-mm o.d. wounds were created on the backs of *db*/*db* mice (5 mice/10 wounds per group), and then treated with a 25-μL solution of **Tβrl–CMP** (0.080–50 mM) for 30 min. The mice were allowed to recover, and the wounds were analyzed after 12 days. The amount of newly formed collagen in the wound bed was identified with picrosirius red stain and expressed as a percentage of the marked area at a depth of 0.75 mm from the healed surface.

The extent to which collagen was deposited was comparable in the wounds treated with 0.08, 0.4, 2.0, and 10.0 mM solutions but increased in wounds treated with 50 mM **Tβrl–CMP** (Figure 5A). These data were mirrored in histopathological analyses (Figure 6).

Wound re-epithelialization did not exhibit a marked dependence on **Tβrl–CMP** dose, though there seemed to be a tendency for a higher response upon treatment with higher doses (Figure 5B). The inflammatory response showed the presence of mononuclear cells in larger amounts in wounds treated with higher doses than in wounds treated with lower doses, which retained discernible amounts of neutrophils and polymorphonuclear cells.

CONCLUSIONS

A **Tβrl–CMP** conjugate can upregulate collagen formation in mice. This result along with in vitro data[21,22] are consistent with its clustering of TGF-β receptors and thereby sensitizing cells to endogenous TGF-β. This mode of action is unique for a pendant on a CMP that is annealed to a wound bed and provides opportunities. The closure of severe wounds where viable tissue has been destroyed by trauma involves the deposition of new collagen in accordance with the severity of the damage. The amplified TGF-β activity during the initial stages of the wound healing process stimulates fibroblast proliferation and activity, as well as keratinocyte migration over the surface of the wounds. This action accelerates the closure of wounds and the acquisition of tensile strength. Dose–response studies suggest that the amount of collagen deposition can be regulated without substantial changes in the rate of re-epithelialization. This type of healing could elicit scar formation but could provide an effective means to treat severe damage, as incurred from third- or fourth-degree burns or traumatic mechanical damage, which might otherwise lead to lifelong impairment.

EXPERIMENTAL PROCEDURES

Materials.

Commercial chemicals were of reagent grade or better, and were used without further purification. Anhydrous solvents were obtained from CYCLE-TAINER solvent delivery systems from J. T. Baker. High-performance liquid chromatography (HPLC)-grade solvents were obtained in sealed bottles from Fisher Chemical. In all reactions involving anhydrous solvents, glassware was either oven- or flame-dried. Polyethylene glycol 8000 (PEG) from Fisher Chemical and bacteriostatic saline (0.9% w/v sodium chloride) from Hospira were used to prepare 5% w/v PEG in saline solution as a delivery vehicle for treatments.

Male mice (n = 92) (BKS.Cg-*Dock7*^{m} +/+ *Lepr*^{db}/J) were from The Jackson Laboratory. Isoflurane was from Abbott Laboratories, buprenorphine·HCl was from Reckitt Benckiser, and chlorhexidine gluconate (4% w/v) was from Purdue Products. Silicone O-rings (15 mm o.d., 11 mm i.d., 2 mm thickness) were from McMaster Carr.

Instrumentation.

Semi-preparative HPLC was performed using a Varian Dynamax C-18 reversed-phase column. Analytical HPLC was performed using a Vydac C-18 reversed-phase column. Mass spectrometry was performed using an Applied Biosystems Voyager DE-Pro matrix-assisted laser desorption/ionization mass spectrometer from Life Technologies at the Biophysics Instrumentation Facility at the University of Wisconsin–Madison.

Peptide Synthesis and Purification.

Peptides were synthesized by SPPS using a 12-channel Symphony peptide synthesizer from Protein Technologies at the University of Wisconsin–Madison Biotechnology Center. Peptides were synthesized on Novabiochem FmocGly-Wang resin (0.4–0.7 mmol g^{-1}, 100–200 mesh) from EMD Chemicals. Amino acids were converted to active esters by treatment with 1-hydroxybenzotriazole (HOBt, 3 equiv), *O*-benzotriazole-*N,N,N′,N′*-tetramethyl-uronium-hexafluoro-phosphate (HBTU, 3 equiv), and *N*-methylmorpholine (NMM, 6 equiv). Fmoc-deprotection was achieved by treatment with piperidine (20% v/v) in dimethylformamide.

CMP and **Tβrl–CMP** were synthesized by the sequential coupling of FmocProOH and FmocProProGlyOH. A proline residue was coupled to the FmocGly-Wang resin after a swell cycle, and the next seven residues were installed by using excess (5 equiv) FmocProOH, FmocProProGlyOH (which was synthesized as reported previously[79]), FmocAsn(Trt)OH, FmocArg(Pbf)OH, FmocHis(Trt)OH, FmocPheOH, FmocMetOH, FmocLys(Boc)OH, FmocGlyOH, FmocThr(*t*Bu)OH, and FmocLeuOH. **CMP** was cleaved from the resin by using 95:2.5:2.5 trifluoroacetic acid (TFA)/triisopropylsilane/water (total volume: 2 mL); **Tβrl–CMP** was cleaved from the resin by using 92.5:5:2.5 TFA/thioanisole/ethanedithiol (total volume: 2 mL). Both peptides were precipitated from *t*-butylmethylether at 0 °C, isolated by centrifugation, and purified by semi-preparative HPLC using linear gradients: **CMP**, 5–85% v/v B over 45 min and **Tβrl–CMP**, 10–90% v/v B over 50 min. Solvent A was H_2O containing TFA (0.1% v/v); solvent B was CH_3CN containing TFA (0.1% v/v). **CMP** was readily soluble in water, but **Tβrl–CMP** required the addition of CH_3CN (20% v/v) to form a clear solution for HPLC analysis. All peptides were judged to be >90% pure by HPLC and matrix-assisted laser desorption/ionization time-of-flight MALDI–TOF mass spectrometry: (m/z) $[M + H]^+$ calcd for **CMP**, 1777; found 1777; (m/z) $[M + H]^+$ calcd for **Tβrl–CMP**, 3221; found 3221.

Tβrl was either obtained from Biomatik or synthesized at the Peptide Synthesis Facility on Fmoc-Asn(Trt)-Wang resin (0.54 mmol g^{-1}, 100–200 mesh; Novabiochem®, EMD Chemicals).

Mouse Models.

Mice aged 8–12 weeks were housed in groups until the day of surgery and then in separate cages post-surgery. The experimental protocol followed was according to the guidelines issued by the Institutional Animal Care and Use Committee at the University of Wisconsin–Madison. Mice were provided food and water *ad libitum*, as well as enrichment, and housed in a temperature-controlled environment with 12-h light and dark cycles.

On the day of the surgery, mice were anaesthetized with isoflurane gas using an induction chamber. For pain management, buprenorphine·HCl (0.01 mg mL^{-1} in 0.9% w/v saline) was injected subcutaneously (0.4 mL per mouse). Eyes were lubricated, and hind nails were clipped. The craniodorsal region was shaved using electric clippers, and the shaved area was scrubbed with alternating cotton swabs of chlorhexidine and sterile saline in circular strokes. Residual hair was removed. For the unsplinted wound model, identical 8-mm wounds were created on each side of the body with a biopsy punch, and the wounding was completed using forceps and scissors to prevent the punch from lacerating the subcutaneous tissue. The wounds were treated with **Tβrl–CMP** or controls, and then allowed to incubate for 30 min while the mouse was still under anesthesia. Wounds were photographed, and the mice were then allowed to recover in their cages. For the dose–response experiments, unsplinted wounds were created with a 6-mm biopsy punch and then treated with 25 μL of the delivery vehicle containing increasing concentrations of **Tβrl–CMP**, followed by incubation for 30 min under anesthesia.

For the splinted-wound model, splints were bilaterally placed in a symmetrical arrangement using an adhesive and then secured to the skin using eight interrupted 5–0 nylon sutures, encircling the splints with the knots.[80] Wounds were created in the center of the splints using an 8-mm biopsy punch and then removing the skin using forceps and scissors. The wounds were then treated with **Tβrl–CMP** or controls, and allowed to incubate for 30 min while the mouse was still under anesthesia. The wounds were photographed, and the mice were allowed to recover on a warming pad. ImageJ software[81] from the National Institutes of Health was used to calculate the wound area (mm^2) from digital photographs. Wound closure was defined as the reduction in the area between the wound edges over the course of the study and was reported as a percentage of the original wound size.

Mice were monitored daily for behavioral changes, and their body weights were recorded on days 1, 3, 6, 9, 12, and 16. The splints were checked daily, and any broken or untied suture was replaced according to the experimental protocol (*vide supra*). If only one suture was compromised during a 24-h period, it was replaced with a new suture. If, however, two or more sutures were compromised during a 24-h period, the wound was no longer considered splinted and was removed from the study.

Wound Harvesting.

Histopathology cassettes were labeled for mouse and wound identification. Note cards (1 in. × 1 in. square) were fitted to the bottom of the histopathology cassettes, and one edge was labeled “cranial” and aligned with the cranial side of the harvested wound. On the final day of the experiment, mice were euthanized using Beuthanasia-D (0.5 mL per mouse). Using

a scalpel blade and scissors, a ¾ in. × ¾ in. square area of the tissue was taken from the mouse, keeping the wound centered in the tissue section. Deep dissection was performed to harvest several layers of tissue deep in the wound. The square section of tissue was affixed to the note card, with the cranial edge aligned with the labeled edge of the card. The cassettes were then closed and placed in formalin-filled jars for histopathological analysis.

Histopathological Analyses.

After euthanasia, the entire wound bed as well as the intact skin margin >5 mm was excised to the retro-peritoneum. The harvested tissue was fixed in 10% v/v formalin for at least 24 h and then sectioned through the center of the lesion. The center was marked with India ink prior to fixation. Routine paraffin processing was performed, and the tissue samples were sectioned serially at a thickness of 5 μm, ensuring that the center of the lesion was included on the slide. The slides were then stained with hematoxylin and eosin and with picrosirius red. Sections were photographed under a light microscope with a mounted DP72 digital camera from Olympus. The size of the wound, length of re-epithilialization, amount of fibrovascular proliferation in the dermis, and inflammatory response were measured on the slides containing the center of the lesion, and images were analyzed using CellScience Dimension 1.4 software from Olympus. The size of the wound was defined as the area of the wound not covered by an advancing epithelial layer and was calculated by measuring the distance between the opposite free edges of the wound. The length of re-epithelialization was defined as the length of the layer of proliferating keratinocytes covering the wound area and was calculated by measuring the distance between the free edge of the keratinocyte layer and the base where the cells were still associated with the native dermal tissue. Both sides of the lesion were measured, and the final result was the sum of the two measurements. For wounds that had undergone complete re-epithelialization, a single measurement was taken from base to base.

Fibrovascular dermal proliferation was measured by examining the picrosirius red-stained sections under polarized light, which highlighted the newly deposited dermal collagen. CellScience Dimension 1.4 software was used to select the wound bed; the amount of new collagen in the selected area was measured and expressed as a percentage of the total wound area or using a semi-quantitative histopathological 0–4 scoring system, where 0 indicated no discernible collagen formation, 1 indicated that <25% of the wound area was covered with fresh collagen, 2 indicated that 25–50% of the wound area was covered with fresh collagen; 3 indicated that 50–75% of the wound area was covered with fresh collagen, and 4 indicated that >75% of the wound area was covered with fresh collagen. The inflammatory response was assessed using a semi-quantitative histopathological 0–4 scoring system, where 0 indicated no inflammation, 1 indicated that <25% of the wound area was affected, 2 indicated that 25–50% of the wound area was affected, 3 indicated that 50–75% of the wound area was affected, and 4 indicated that >75% of the wound area was affected. The inflammatory response was also categorized as “acute” when >75% of the cells were neutrophils; “chronically active” when there was a 1:1 ratio of neutrophils and mononuclear cells; and “chronic” when >75% of the inflammatory cells were mononuclear.

Statistical Analyses.

All data were analyzed using a Mann–Whitney rank sum test, and statistical significance was set to $p < 0.05$. Statistical analyses were executed using Prism Version 5.0 software from GraphPad Software.

ACKNOWLEDGMENTS

We are grateful to L. Li and N. L. Abbott for their guidance and advice. We thank P. Kierski, D. Calderon, D. Tackes, K. Johnson, and Z. Joseph for help with the wound surgery and animal care.

Funding

This work was supported by grants RC2 AR058971, R56 AR044276, R01 AI055258, and R01 GM049975 (NIH). MALDI–TOF mass spectrometry was performed at the University of Wisconsin–Madison Biophysics Instrumentation Facility, which was established with Grants BIR-9512577 (NSF) and S10 RR013790 (NIH).

ABBREVIATIONS

CMP	collagen-mimetic peptide (here, $(PPG)_7$)
TGF-β	transforming growth factor-β
Tβrl–CMP	collagen-mimetic peptide–transforming growth factor-β receptor ligand conjugate (here, LTGKNFPMFHRN–$(PPG)_7$)
TβRI	transforming growth factor-β type-1 receptor
TβRII	transforming growth factor-β type-2 receptor
Tβrl	transforming growth factor-β receptor ligand (here, LTGKNFPMFHRN)

REFERENCES

(1). Massagué J TGF-β signal transduction. Annu. Rev. Biochem 1998, 67, 753–791. [PubMed: 9759503]

(2). Shi Y; Massagué J Mechanisms of TGF-β signaling from cell membrane to the nucleus. Cell 2003, 113, 685–700. [PubMed: 12809600]

(3). Massagué J TGF β signalling in context. Nat. Rev. Mol. Cell Biol 2012, 13, 613–630.

(4). Meng X.-m.; Nikolic-Paterson DJ; Lan HY TGF-β: The master regulator of fibrosis. Nat. Rev. Nephrol 2016, 12, 325–338. [PubMed: 27108839]

(5). Wrana JL; Attisano L; Cárcamo J; Zentella A; Doody J; Laiho M; Wang X-F; Massague J TGF-β signals through a heteromeric protein kinase receptor complex. Cell 1992, 71, 1003–1014. [PubMed: 1333888]

(6). Hart PJ; Deep S; Taylor AB; Shu Z; Hinck CS; Hinck AP Crystal structure of the human TβR2 ectodomain–TGFβ3 complex. Nat. Struct. Mol. Biol 2002, 9, 203–208.

(7). Heldin C-H; Moustakas A Signaling receptors for TGF-β family members. Cold Spring Harb. Prospect. Biol 2016, 8, a022053.

(8). Schiller M; Javelaud D; Mauviel A TGF-β-induced SMAD signaling and gene regulation: Consequences for extracellular matrix remodeling and wound healing. J. Dermatol. Sci 2004, 35, 83–92. [PubMed: 15265520]

(9). Faler BJ; Macsata RA; Plummer D; Mishra L; Sidawy AN Transforming growth factor-β and wound healing. Persp. Vasc. Surg. Endovasc. Ther 2006, 18, 55–62.

(10). Prud'homme GJ Pathobiology of transforming growth factor β in cancer, fibrosis and immunologic disease, and therapeutic considerations. Lab. Invest 2007, 87, 1077–1091. [PubMed: 17724448]

(11). Pakyari M; Farrokhi A; Maharlooei MK; Ghahary A Critical role of transforming growth factor beta in different phases of wound healing. Adv. Wound Care (New Rochelle) 2013, 2, 215–224. [PubMed: 24527344]

(12). Liarte S; Bernabé-García Á; Nicolás FJ Role of TGF-β in skin chronic wounds: A keratinocyte perspective. Cells 2020, 9, 306.

(13). Henderson NC; Rieder F; Wynn TA Fibrosis: From mechanisms to medicines. Nature 2020, 587, 555–566. [PubMed: 33239795]

(14). Pandit A; Ashar A; Feldman D The effect of TGF-β delivered through a collagen scaffold on wound healing. J. Invest. Surg 1999, 12, 89–100. [PubMed: 10327078]

(15). Mustoe T; Pierce G; Thomason A; Gramates P; Sporn M; Deuel T Accelerated healing of incisional wounds in rats induced by transforming growth factor-β. Science 1987, 237, 1333–1336. [PubMed: 2442813]

(16). Broadley KN; Aquino AM; Hicks B; Ditesheim JA; McGee GS; Demetriou AA; Woodward SC; Davidson JM The diabetic rat as an impaired wound healing model: Stimulatory effects of transforming growth factor-β and basic fibroblast growth factor. Biotechnol. Ther 1989, 1, 55–68. [PubMed: 2562644]

(17). Ammann AJ; Beck LS; DeGuzman LEO; Hirabayashi SE; Pun Lee W; McFatridge L; Nguyen TUE; Xu Y; Mustoe TA Transforming growth factor-β effect on soft tissue repair. Ann. N.Y. Acad. Sci 1990, 593, 124–134. [PubMed: 2375591]

(18). Ksander GA; Chu GH; McMullin H; Ogawa Y; Pratt BM; Rosenblatt JS; McPherson JM Transforming growth factors-β1 and β2 enhance connective tissue formation in animal models of dermal wound healing by secondary intent. Ann. N.Y. Acad. Sci 1990, 593, 135–147. [PubMed: 2375592]

(19). Ksander GA; Gerhardt CO; Olsen DR Exogenous transforming growth factor-β2 enhances connective tissue formation in transforming growth factor-β1—deficient, healing-impaired dermal wounds in mice. Wound Rep. Regen 1993, 1, 137–148.

(20). Beck LS; DeGuzman L; Lee WP; Xu Y; Siegel MW; Amento EP One systemic administration of transforming growth factor-beta 1 reverses age- or glucocorticoid-impaired wound healing. J. Clin. Invest 1993, 92, 2841–2849. [PubMed: 8254038]

(21). Li L; Orner BP; Huang T; Hinck AP; Kiessling LL Peptide ligands that use a novel binding site to target both TGF-β receptors. Mol. BioSys 2010, 6, 2392–2402.

(22). Li L; Klim JR; Derda R; Courtney AH; Kiessling LL Spatial control of cell fate using synthetic surfaces to potentiate TGF-β signaling. Proc. Natl. Acad. Sci. U.S.A 2011, 108, 11745–11750. [PubMed: 21719709]

(23). Shoulders MD; Raines RT Collagen structure and stability. Annu. Rev. Biochem 2009, 78, 929–958. [PubMed: 19344236]

(24). Chattopadhyay S; Raines RT Collagen-based biomaterials for wound healing. Biopolymers 2014, 101, 821–833. [PubMed: 24633807]

(25). Bella J; Hulmes DJS Fibrillar collagen. Subcell. Biochem 2017, 82, 457–490. [PubMed: 28101870]

(26). Chattopadhyay S; Murphy CJ; McAnulty JF; Raines RT Peptides that anneal to natural collagen in vitro and ex vivo. Org. Biomol. Chem 2012, 10, 5892–5897. [PubMed: 22522497]

(27). Wahyudi H; Reynolds AA; Li Y; Owen SC; Yu SM Targeting collagen for diagnostic imaging and therapeutic delivery. J. Control Release 2016, 240, 323–331. [PubMed: 26773768]

(28). Chattopadhyay S; Gutherie KM; Teixeira L; Murphy CJ; Dubielzig RR; McAnulty JF; Raines RT Anchoring a cytoactive factor in a wound bed promotes healing. J. Tissue Eng. Regen. Med 2016, 10, 1012–1020.

(29). Bennink LL; Li Y; Kim B; Shin IJ; San BH; Zangari M; Yoon D; Yu SM Visualizing collagen proteolysis by peptide hybridization: From 3D cell culture to in vivo imaging. Biomaterials 2018, 183, 67–76. [PubMed: 30149231]

(30). Ellison AJ; Raines RT A pendant peptide endows a sunscreen with water-resistance. Org. Biomol. Chem 2018, 16, 7139–7142. [PubMed: 30256375]

(31). Dones JM; Tanrikulu IC; Chacko JV; Schroeder AB; Hoang TT; Gibson ALF; Eliceiri KW; Raines RT Optimization of interstrand interactions enables burn detection with a collagen-mimetic peptide. Org. Biomol. Chem 2019, 17, 9906–9912. [PubMed: 31720665]

(32). Schroeder AB; Karim A; Ocotl E; Dones JM; Chacko JV; Liu A; Raines RT; Gibson ALF; Eliceiri KW Optical imaging of collagen fiber damage to assess thermally injured human skin. Wound Rep. Regen 2020, 28, 848–855.

(33). Ellison AJ; Tanrikulu IC; Dones JM; Raines RT Cyclic peptide mimetic of damaged collagen. Biomacromolecules 2020, 21, 1539–1547. [PubMed: 32159956]

(34). Ellison AJ; Dempwolff F; Kearns DB; Raines RT Role for cell-surface collagen of Streptococcus pyogenes in infections. ACS Infect. Dis 2020, 6, 1836–1843. [PubMed: 32413256]

(35). Song JY; Pineault KM; Dones JM; Raines RT; Wellik DM Hox genes maintain critical roles in the adult skeleton. Proc. Natl. Acad. Sci. U.S.A 2020, 117, 7296–7304. [PubMed: 32170021]

(36). Newberry RW; Raines RT 4-Fluoroprolines: Conformational analysis and effects on the stability and folding of peptides and proteins. Top. Hetercycl. Chem 2017, 48, 1–25.

(37). Davidson JM Animal models for wound repair. Arch. Dermatol. Res 1998, 290, (Suppl.): S1–S11. [PubMed: 9710378]

(38). Greenhalgh DG; Warden GD, Wound Care Models. In Surgical Research, Academic Press: London, UK, 2001; pp 379–391.

(39). Zomer HD; Trentin AG Skin wound healing in humans and mice: Challenges in translational research. J. Dermatol. Sci 2018, 90, 3–12. [PubMed: 29289417]

(40). Parnell LKS; Volk SW The evolution of animal models in wound healing research: 1993–2017. Adv. Wound Care (New Rochelle) 2019, 8, 692–702. [PubMed: 31827981]

(41). Coleman D Obese and diabetes: Two mutant genes causing diabetes-obesity syndromes in mice. Diabetologia 1978, 14, 141–148. [PubMed: 350680]

(42). Kämpfer H; Paulukat J; Mühl K; Wetzler C; Pfeilschifter J; Frank S Lack of interferon-ν production despite the presence of interleukin-18 during cutaneous wound healing. Mol. Med 2000, 6, 1016–1027. [PubMed: 11474118]

(43). Brem H; Tomic-Canic M; Entero H; Hanflik AM; Wang VM; Fallon JT; Ehrlich HP The synergism of age and db/db genotype impairs wound healing. Exp. Gerontol 2007, 42, 523–531. [PubMed: 17275236]

(44). Michaels J; Churgin SS; Blechman KM; Greives MR; Aarabi S; Galiano RD; Gurtner GC db/db Mice exhibit severe wound-healing impairments compared with other murine diabetic strains in a silicone-splinted excisional wound model. Wound Rep. Regen 2007, 15, 665–670.

(45). Greenhalgh DG Wound healing and diabetes mellitus. Clin. Plas. Surg 2003, 30, 37–45.

(46). Werner S; Breeden M; Hubner G; Greenhalgh DG; Longaker MT Induction of keratinocyte growth factor expression is reduced and delayed during wound healing in the genetically diabetic mouse. J. Invest. Dermatol 1994, 103, 469–473. [PubMed: 7930669]

(47). Norido F; Canella R; Zanoni R; Gorio A Development of diabetic neuropathy in the C57BL/Ks (db/db) mouse and its treatment with gangliosides. Exp. Neurol 1984, 83, 221–232. [PubMed: 6692864]

(48). Greenhalgh DG; Sprugel KH; Murray MJ; Ross R PDGF and FGF stimulate wound healing in the genetically diabetic mouse. Am. J. Pathol 1990, 136, 1235–1246. [PubMed: 2356856]

(49). Brown RL; Breeden MP; Greenhalgh DG PDGF and TGF-α act synergistically to improve wound healing in the genetically diabetic mouse. J. Surg. Res 1994, 56, 562–570. [PubMed: 8015312]

(50). Dapson RW; Fagan C; Kiernan JA; Wickersham TW Certification procedures for sirius red F3B (CI 35780, Direct red 80). Biotech. Histochem 2011, 86, 133–139. [PubMed: 21417582]

(51). Postlethwaite AE; Keski-Oja J; Moses HL; Kang AH Stimulation of the chemotactic migration of human fibroblasts by transforming growth factor β. J. Exp. Med 1987, 165, 251–256. [PubMed: 3491869]

(52). Ashcroft GS; Yang X; Glick AB; Weinstein M; Letterio JJ; Mizel DE; Anzano M; Greenwell-Wild T; Wahl SM; Deng C; Roberts AB Mice lacking Smad3 show accelerated wound healing and an impaired local inflammatory response. Nat. Cell Biol 1999, 1, 260–266. [PubMed: 10559937]

(53). Abe R; Donnelly SC; Peng T; Bucala R; Metz CN Peripheral blood fibrocytes: Differentiation pathway and migration to wound sites. J. Immunol 2001, 166, 7556–7562. [PubMed: 11390511]

(54). Lal BK; Saito S; Pappas PJ; Padberg FT; Cerveira JJ; Hobson RW; Durán WN Altered proliferative responses of dermal fibroblasts to TGF-β1 may contribute to chronic venous stasis ulcer. J. Vasc. Surg 2003, 37, 1285–1293. [PubMed: 12764277]

(55). Roberts CJ; Birkenmeier TM; McQuillan JJ; Akiyama SK; Yamada SS; Chen WT; Yamada KM; McDonald JA Transforming growth factor β stimulates the expression of fibronectin and of both subunits of the human fibronectin receptor by cultured human lung fibroblasts. J. Biol. Chem 1988, 263, 4586–4592. [PubMed: 2965146]

(56). Lynch SE; Colvin RB; Antoniades HN Growth factors in wound healing. Single and synergistic effects on partial thickness porcine skin wounds. J. Clin. Invest 1989, 84, 640–646. [PubMed: 2788174]

(57). Roberts AB; Sporn MB; Assoian RK; Smith JM; Roche NS; Wakefield LM; Heine UI; Liotta LA; Falanga V; Kehrl JH Transforming growth factor type β: Rapid induction of fibrosis and angiogenesis in vivo and stimulation of collagen formation in vitro. Proc. Natl. Acad. Sci. U.S.A 1986, 83, 4167–4171. [PubMed: 2424019]

(58). Roberts AB Transforming growth factor-β: activity and efficacy in animal models of wound healing. Wound Rep. Regen 1995, 3, 408–418.

(59). Roberts AB; Piek E; Böttinger EP; Ashcroft G; Mitchell JB; Flanders KC Is Smad3 a major player in signal transduction pathways leading to fibrogenesis? Chest 2001, 120, S43–S47.

(60). Schmid P; Itin P; Cherry G; Bi C; Cox DA Enhanced expression of transforming growth factor-β type I and type II receptors in wound granulation tissue and hypertrophic scar. Am. J. Pathol 1998, 152, 485–493. [PubMed: 9466575]

(61). Mann BK; Schmedlen RH; West JL Tethered-TGF-β increases extracellular matrix production of vascular smooth muscle cells. Biomaterials 2001, 22, 439–444. [PubMed: 11214754]

(62). Mann BK; Tsai AT; Scott-Burden T; West JL Modification of surfaces with cell adhesion peptides alters extracellular matrix deposition. Biomaterials 1999, 20, 2281–2286. [PubMed: 10614934]

(63). Slevin M; Krupinski J; Slowik A; Kumar P; Szczudlik A; Gaffney J Serial measurement of vascular endothelial growth factor and transforming growth factor-β1 in serum of patients with acute ischemic stroke. Stroke 2000, 31, 1863–1870. [PubMed: 10926948]

(64). Kane CJM; Hebda PA; Mansbridge JN; Hanawalt PC Direct evidence for spatial and temporal regulation of transforming growth factor β1 expression during cutaneous wound healing. J. Cell. Physiol 1991, 148, 157–173. [PubMed: 1907288]

(65). Wang X-J; Han G; Owens P; Siddiqui Y; Li AG Role of TGFβ-mediated inflammation in cutaneous wound healing. J. Invest. Dermatol. Symp. Proc 2006, 11, 112–117.

(66). Wahl SM; Hunt DA; Wakefield LM; McCartney-Francis N; Wahl LM; Roberts AB; Sporn MB Transforming growth factor type beta induces monocyte chemotaxis and growth factor production. Proc. Natl. Acad. Sci. U.S.A 1987, 84, 5788–5792. [PubMed: 2886992]

(67). Tsunawaki S; Sporn M; Ding A; Nathan C Deactivation of macrophages by transforming growth factor-β. Nature 1988, 334, 260–262. [PubMed: 3041283]

(68). Edwards DR; Murphy G; Reynolds JJ; Whitham SE; Docherty AJ; Angel P; Heath JK Transforming growth factor β modulates the expression of collagenase and metalloproteinase inhibitor. EMBO J. 1987, 6, 1899–1904. [PubMed: 2820711]

(69). Rousselle P; Braye F; Dayan G Re-epithelialization of adult skin wounds: Cellular mechanisms and therapeutic strategies. Adv. Drug Deliv. Rev 2019, 146, 344–365. [PubMed: 29981800]

(70). Badiavas EV; Zhou L; Falanga V Growth inhibition of primary keratinocytes following transduction with a novel TGFβ-1 containing retrovirus. J. Dermatol. Sci 2001, 27, 1–6. [PubMed: 11457637]

(71). Jeong H-W; Kim I-S TGF-β1 enhances βig-h3-mediated keratinocyte cell migration through the α3β1 integrin and PI3K. J. Cell. Biochem 2004, 92, 770–780. [PubMed: 15211574]

(72). Tredget EB; Demare J; Chandran G; Tredget EE; Yang L; Ghahary A Transforming growth factor-β and its effect on reepithelialization of partial-thickness ear wounds in transgenic mice. Wound Rep. Regen 2005, 13, 61–67.

(73). Lu L; Saulis AS; Liu WR; Roy NK; Chao JD; Ledbetter S; Mustoe TA The temporal effects of anti–TGF-β1, 2, and 3 monoclonal antibody on wound healing and hypertrophic scar formation. J. Am. Coll. Surg 2005, 201, 391–397. [PubMed: 16125072]

(74). Ashcroft GS; Roberts AB Loss of Smad3 modulates wound healing. Cytokine Growth Factor Rev. 2000, 11, 125–131. [PubMed: 10708960]

(75). Galiano RD; Michaels VJ; Dobryansky M; Levine JP; Gurtner GC Quantitative and reproducible murine model of excisional wound healing. Wound Rep. Regen 2004, 12, 485–492.

(76). Hebda PA Stimulatory effects of transforming growth factor-β and epidermal growth factor on epidermal cell outgrowth from porcine skin explant cultures. J. Invest. Dermatol 1988, 91, 440–445. [PubMed: 3262693]

(77). Hebda PA The acceleration of epidermal wound healing in partial thickness burns by transforming growth factor-beta. J. Invest. Dermatol 1989, 92, 442.

(78). Gailit J; Welch MP; Clark RAF TGF-β1 stimulates expression of keratinocyte integrins during re-epithelialization of cutaneous wounds. J. Invest. Dermatol 1994, 103, 221–227. [PubMed: 8040614]

(79). Jenkins CL; Vasbinder MM; Miller SJ; Raines RT Peptide bond isosteres: Ester or (E)-alkene in the backbone of the collagen triple helix. Org. Lett 2005, 7, 2619–2622. [PubMed: 15957905]

(80). Galiano RD; Michaels J 5th; Dobryansky M; Levine JP; Gurtner GC Quantitative and reproducible murine model of excisional wound healing. Wound Rep. Regen 2004, 12, 485–492.

(81). Schroeder AB; Dobson ETA; Rueden CT; Tomancak P; Jug F; Eliceiri KW The ImageJ ecosystem: Open-source software for image visualization, processing, and analysis. Protein Sci. 2021, 30, 234–249. [PubMed: 33166005]

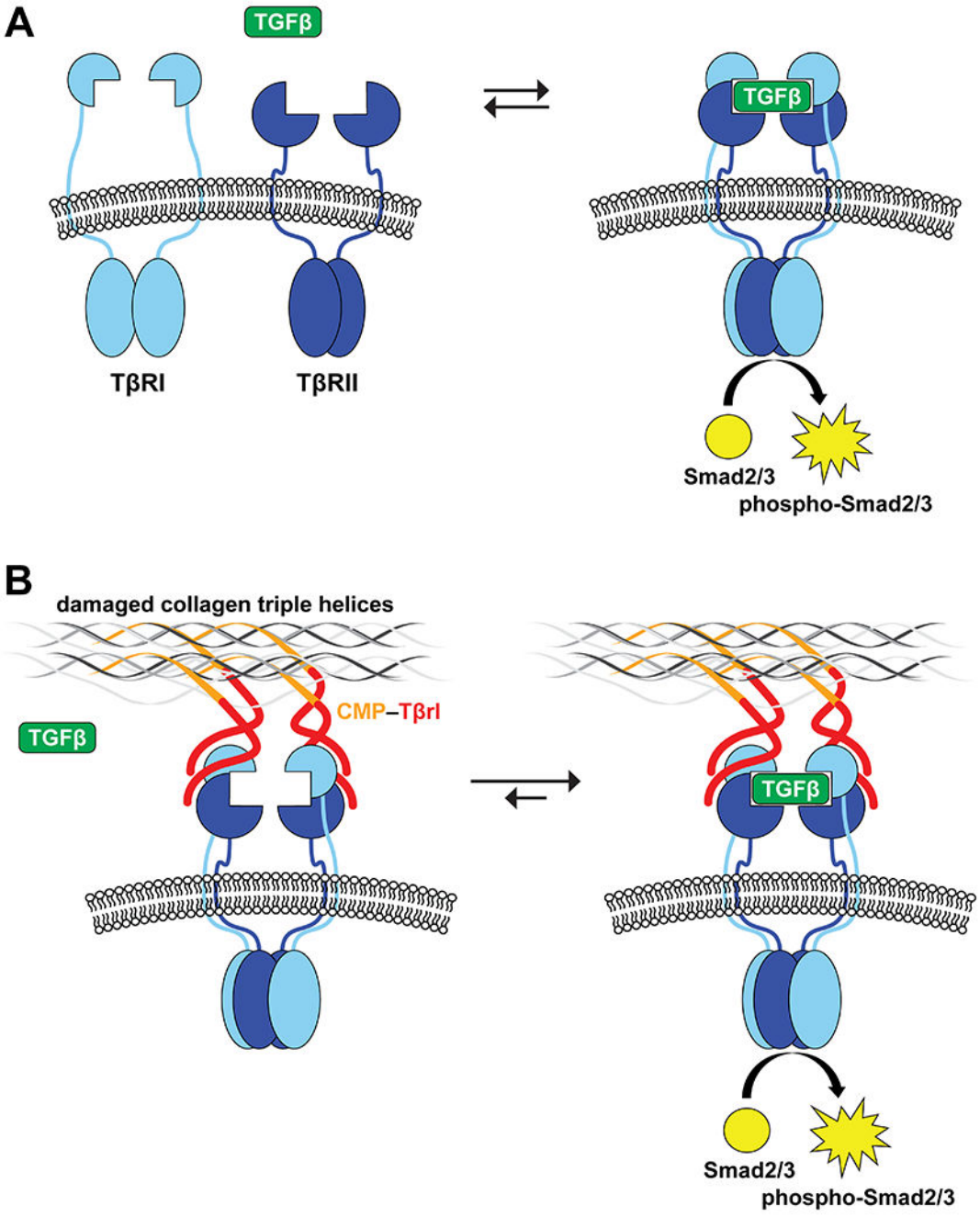

Figure 1.

Representation of TGF-β receptor–ligand complex formation and its activation of the Smad2/3 proteins by their cytosolic kinase domains. (A) TGF-β induces the heterotetramerization of type-I and type-II receptors (TβRI and TβRII). (B) Clustering of TβRI and TβRII by binding to a ligand (**Tβrl**) that is immobilized in a wound bed upon the annealing of a pendant **CMP**.

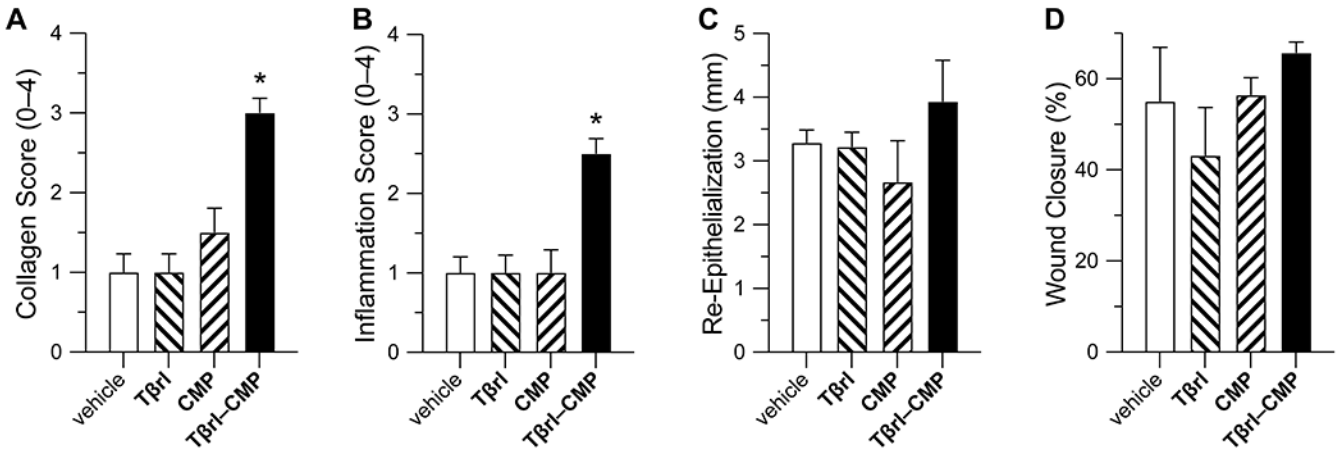

Figure 2.

Effect of **TβrI–CMP** (0.5 μmol) and controls on the healing of unsplinted cutaneous wounds in mice. Values are the mean ± SE ($n = 10$ wounds in 5 mice) with $*p < 0.05$. (A) Fibrovascular influx in wounds on a scale of 0–4 on day 12 post-surgery. (B) Inflammation in wounds on a scale of 0–4 on day 12 post-surgery. (C) Re-epithelialization of wounds on day 16 post-surgery. (D) Wound closure by day 12 post-surgery, calculated as the wound size as a percentage of the original wound size on day 0.

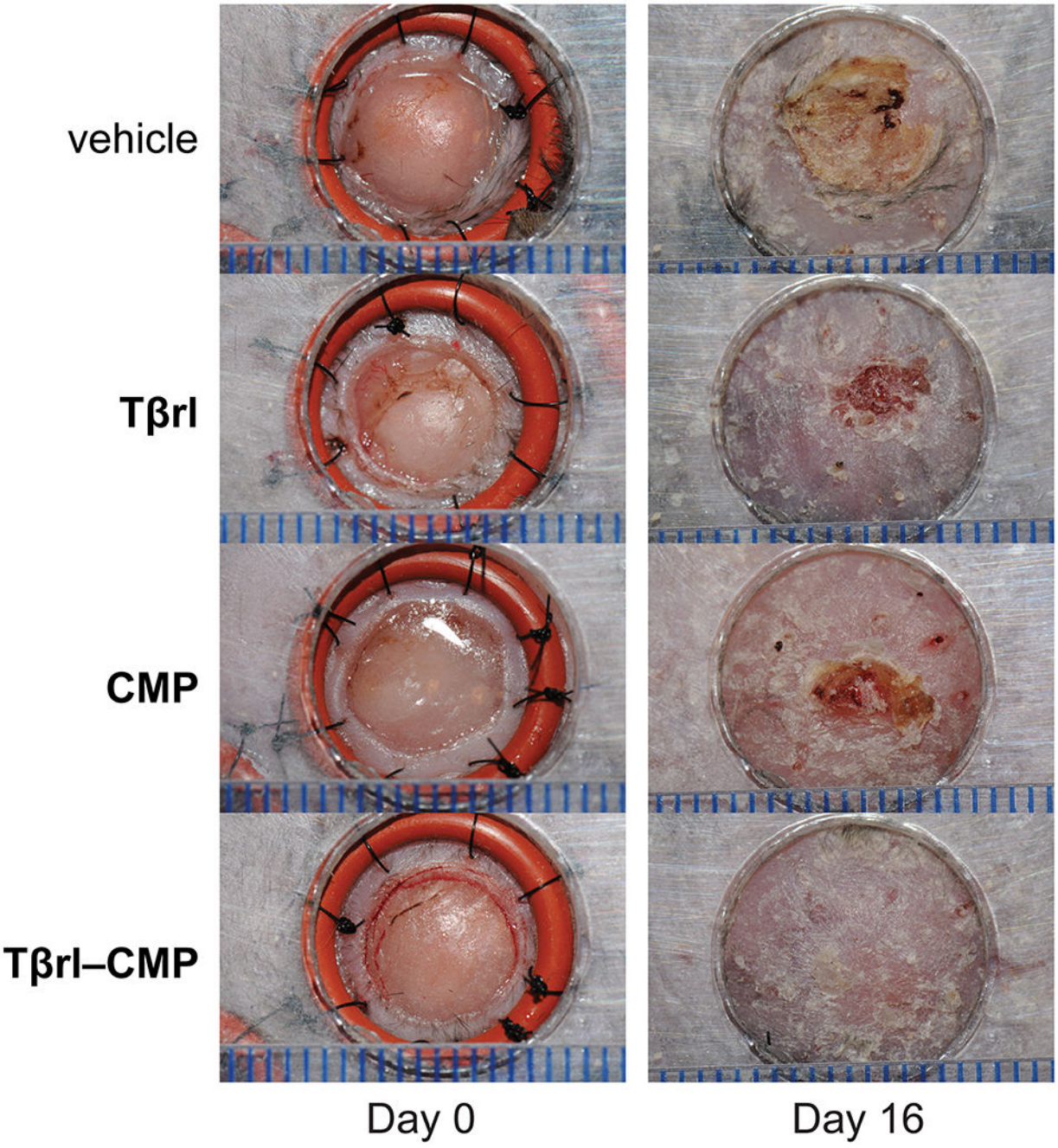

Figure 3.

Representative images of splinted wounds in mice on day 0 (*i.e.*, immediately post-surgery) and on day 16 post-surgery after the removal of splints but before euthanasia. Wounds were treated with vehicle (5% PEG/saline), **TβrI** (0.5 μmol), **CMP** (0.5 μmol), or **TβrI–CMP** (0.5 μmol). In mice treated with **TβrI–CMP,** 15 of the 16 wounds showed complete closure. Scale bars (blue) are separated by 1.0 mm.

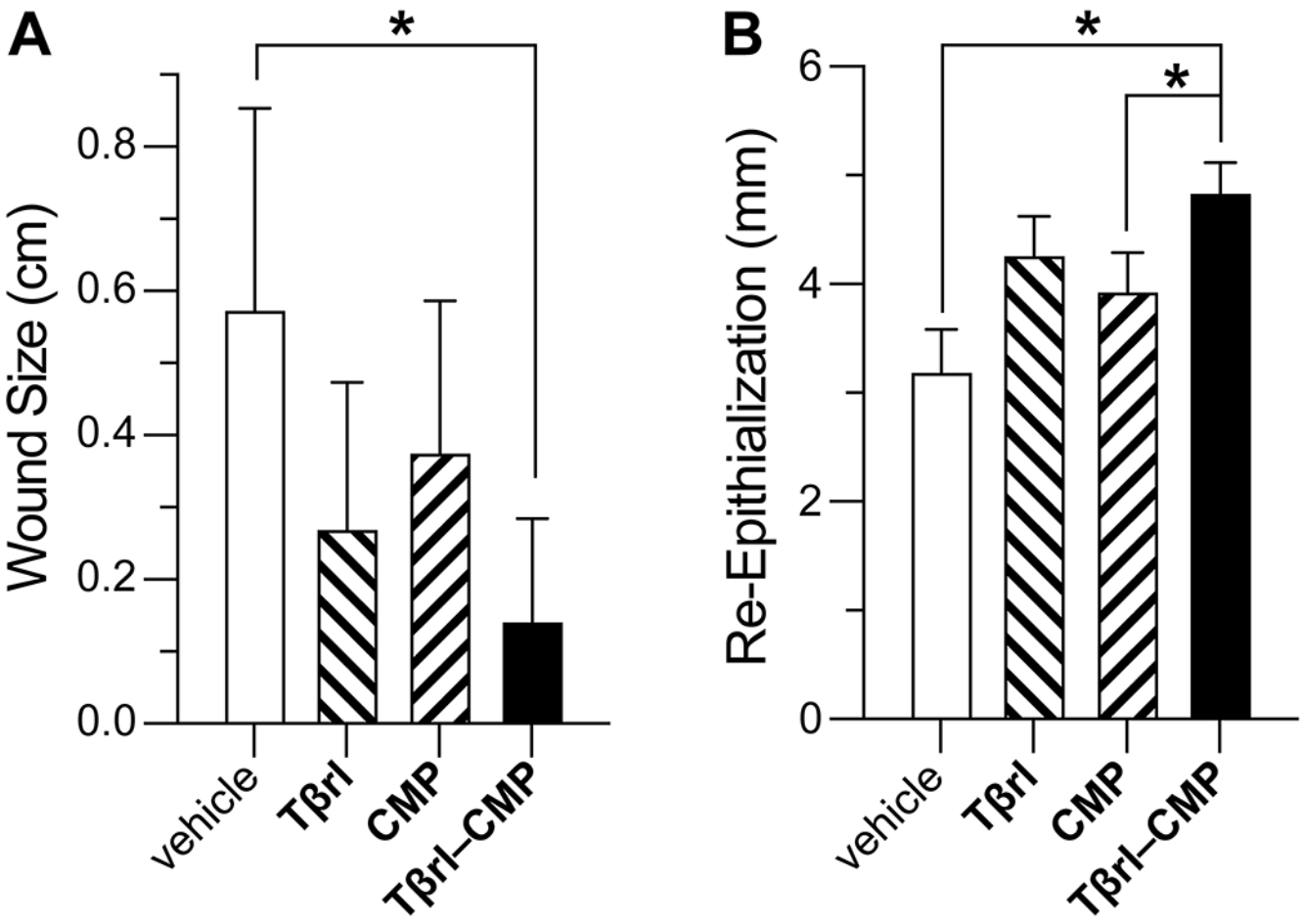

Figure 4.

Effect of **Tβrl–CMP** (0.5 μmol) and controls on the healing of splinted cutaneous wounds in mice. (A) Wound closure on day 16 post-surgery, represented as the distance between advancing edges at the widest diameter. (B) Re-epithelialization of wounds by day 16 post-surgery. Values are the mean ± SE (n = 16 wounds in 8 mice) with *$p < 0.05$.

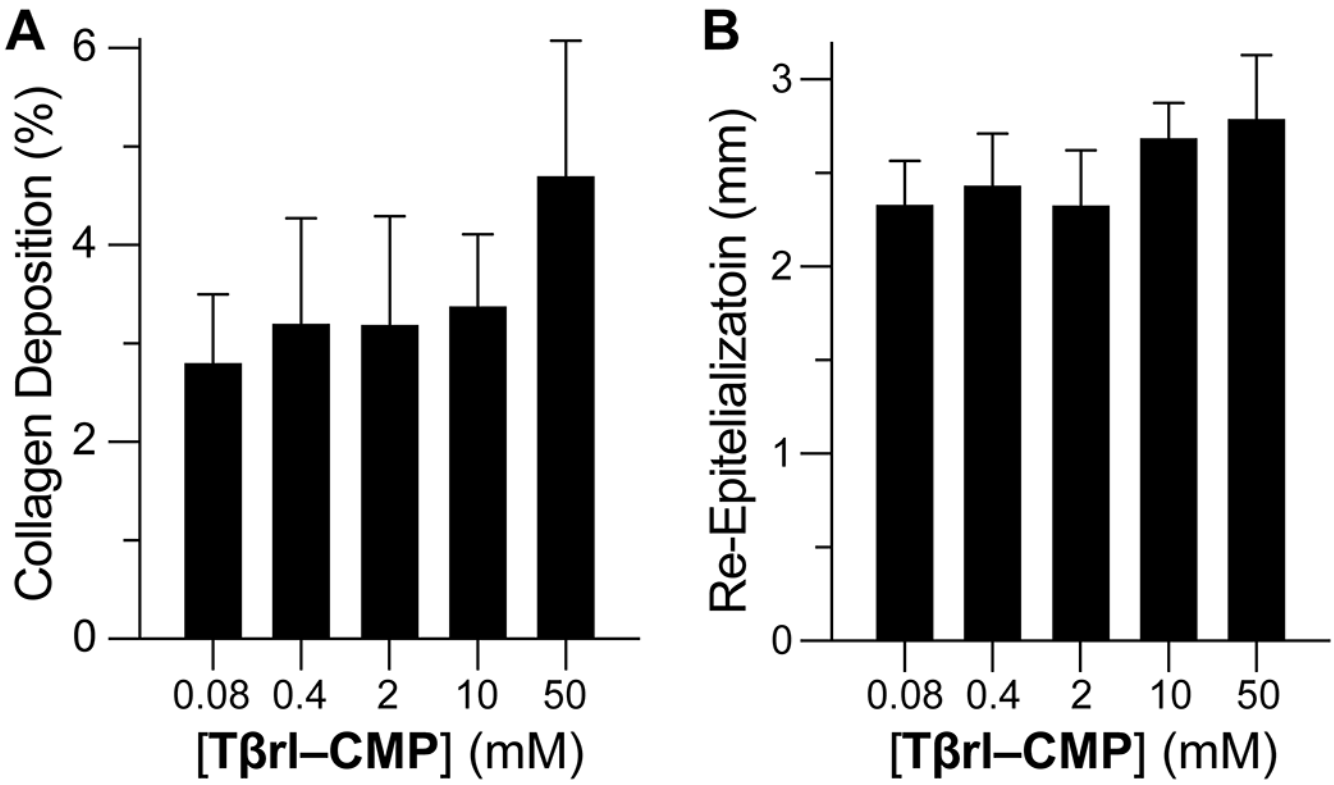

Figure 5.

Dose–response analysis of unsplinted cutaneous wounds in mice to **TβrI–CMP** and controls. Wounds were treated with a 25-μL solution of **TβrI–CMP** in 5% PEG/saline and analyzed on day 12 post-surgery. Values are the mean ± SE (n = 16 wounds in 8 mice). (A) New collagen deposition at a depth of 0.75 mm from the healed surface. (B) Re-epithelialization of wounds.

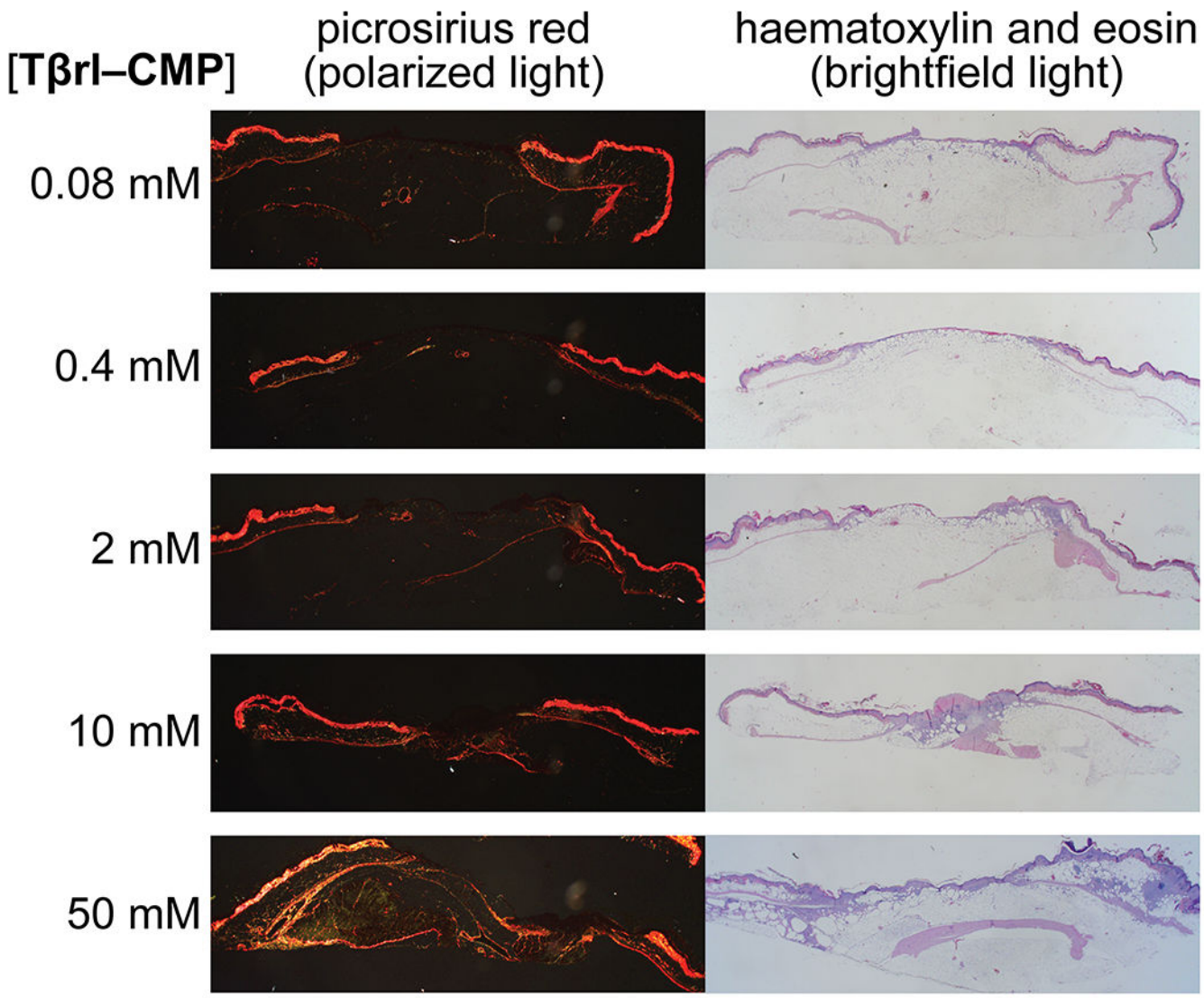

Figure 6.

Representative histological images of **TβrI–CMP**-treated wounds on day 12 post-surgery. Wounds were stained with picrosirius red and imaged with polarized light or with hematoxylin and eosin and imaged with brightfield light.